Journal of Porphyrins and Phthalocyanines
J. Porphyrins Phthalocyanines 2012; **16**: 140–148
DOI: 10.1142/S108842461200446X

Published at http://www.worldscinet.com/jpp/

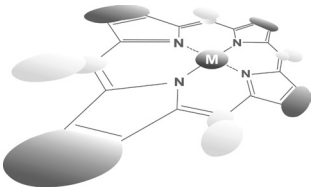

Picosecond and femtosecond optical nonlinearities of novel corroles

Syed Hamad[a], Surya P. Tewari[a,b], L. Giribabu[c] and S. Venugopal Rao*[b]

[a]*School of Physics, University of Hyderabad, Hyderabad 500046, India*
[b]*Advanced Centre of Research in High Energy Materials (ACRHEM), University of Hyderabad, Hyderabad 500046, India*
[c]*Inorganic & Physical Chemistry Division, Indian Institute of Chemical Technology, Hyderabad 50007, India*

Received 24 August 2011
Accepted 5 October 2011

ABSTRACT: We present our results from the experimental and modeling studies of picosecond (ps) and femtosecond (fs) nonlinearities of two novel corroles (a) tritolyl corrole (TTC) (b) triphenyl corrole (TPC) using the Z-scan technique. Both open and closed aperture Z-scan curves were recorded with ~2 ps/~40 fs laser pulses at a wavelength of 800 nm and nonlinear optical coefficients were extracted for both studies. Both the molecules possessed negative nonlinear refractive index (n_2) as revealed by signature of the closed aperture data in both (ps and fs) time domains. Picosecond nonlinear absorption data of TPC obtained at a concentration of 5×10^{-4} M demonstrated complex behavior with switching from reverse saturable absorption (RSA) within saturable absorption (SA) at lower peak intensities to RSA at higher peak intensities. TTC data recorded at the similar concentration exhibited saturable absorption (SA) type of behavior at lower peak intensities to switching from RSA with in SA at higher peak intensities. At a concentration of 2.5×10^{-4} M, the ps open aperture data at higher peak intensities illustrated effective three-photon absorption (3PA) for both the molecules. We also report the picosecond spectral dependent Z-scan studies performed at 680 nm, 700 nm, and 740 nm. Nonlinear absorption and refraction of both the samples at these three wavelengths were studied in detail. Femtosecond nonlinear absorption data of TPC and TTC demonstrated the behavior of saturable absorption (SA) at a concentration of 1×10^{-3} M. Solvent contribution to the nonlinearity was also identified. We have also evaluated the sign and magnitude of third order nonlinearity. We discuss the nonlinear optical performance of these organic molecules.

KEYWORDS: picosecond, femtosecond, saturable absorption, effective three photon absorption.

INTRODUCTION

Porphyrins, phthalocyanines, and porphycenes are macromolecules with huge number of delocalized π electrons resulting in interesting third order nonlinear optical (NLO) properties leading to extensive applications in optical limiting, all-optical switching, and optical signal processing [1–6]. Corroles are tetrapyrrolic molecules maintaining the skeletal structure of Corrin with its three *meso* carbon positions and one direct pyrrole-pyrrole linkage and possessing the aromaticity of porphyrins [7–12]. Corroles generally show porphyrin type spectra, with strong absorptions in the visible range associated with very highly colored compounds. Moreover, among the interesting attributes of corroles are their photo physical properties. As well, the direct pyrrole–pyrrole linkage seems to give corroles stronger fluorescence properties than their porphyrin counterparts. These properties open up potential for using corroles in many applications, including diverse areas such as cancer diagnosis, treatment, and

*Correspondence to: S. Venugopal Rao, email: svrsp@uohyd.ernet.in and soma_venu@yahoo.com, tel: +91 040-23138811, fax: +91 040-23012800

solar cell research. Rebane *et al.* [13, 14] studied the NLO properties and reported two-photon absorption (2PA) cross sections and spectra of corroles within a broad spectral range of excitation wavelengths, 800–1400 nm. They also observed that the strength of 2PA peak in the Soret region strongly decreased with the electron-withdrawing ability of the side substituents. Cho *et al.* [15] studied corrole dimers and obtained superior values of two-photon cross-section compared to the values obtained by Rebane *et al.* [13, 14]. Our group has been investigating a number of porphyrins and phthalocyanines for their NLO properties in cw, nanosecond (ns), picosecond (ps) and femtosecond (fs) time domains [16–27]. The motivation for such studies is many fold. For any new molecule synthesized it is imperative to study its NLO properties with different pulse durations and at different wavelengths to identify the resonant and non-resonant contributions to the nonlinearity. A molecule might be useful for optical limiting applications when studied with ns/ps pulses while it's utility for signal processing or all-optical switching is decided by the femtosecond NLO properties and dynamics. A molecule could be applied for broadband optical limiting or could possess interesting NLO properties at different wavelengths and input intensities. Therefore, for identification of the complete potential of any new molecule, studies at different input conditions (wavelengths, pulse duration, input intensity, surrounding matrix etc.) are indispensable. In this paper we present the results of our studies on nonlinear optical properties of triphenyl corrole (TPC) and tritolyl corrole (TTC) with Z-scan technique with ~2 ps and ~40 fs laser pulses excitation at the same 800 nm wave length. We also report here our results on the ps and fs NLO properties of two corroles [triphenyl corrole and tritolyl corrole, herewith represented as TPC and TTC, throughout this script] studied at same wavelength of 800 nm and picosecond spectral dependent studies at the wavelengths of 680 nm, 700 nm, and 740 nm with the standard Z-scan technique. The sign and magnitude of nonlinear refractive index were derived from the closed aperture Z-scan in both ps & fs domains. From the ps nonlinear absorption data, achieved through the open aperture Z-scans, we observed the two photon absorption (0.5 mM solutions) and three photon absorption (0.25 mM solutions). From the fs Z-scan data we deduced saturable absorption as the main nonlinear absorption mechanism and evaluated their third order nonlinearities. Our studies in ps domain provide sufficient evidence that these molecules possess superior nonlinear coefficients required for applications in optical switching.

EXPERIMENTAL

Synthesis of corroles

TPC and TTC were prepared according to the procedure described below [28]. For obtaining TPC benzaldehyde (330 mg, 5 m mol) and pyrrole (670 mg, 10 mM) were dissolved in a mixture of methanol and water (400 mL, 1:1 of methanol:H_2O). To this 4.25 mL of HCl was added and the reaction mixture was stirred at room temperature for 3 h. The reaction mixture was extracted with $CHCl_3$, and the organic layer was washed with H_2O and dried over anhydrous Na_2SO_4. To this *p*-chloranil (1.23 g, 5 mM) was added, and the mixture was refluxed for 1 h. The reaction mixture subjected to silica gel column chromatography and eluted with $CHCl_3$:hexane (1:1 v/v). The solvent front running brown color band was collected and re-crystallized from $CHCl_3$:hexane afforded pure corrole. For the synthesis of TTC *P*-tolylaldehyde (600 mg, 5 mM) and pyrrole (670 mg, 10 mM) were dissolved in a mixture of methanol and water (400 mL, 1:1 of methano:H_2O). To this 4.25 mL of HCl was added, and the reaction mixture was stirred at room temperature for 3 h. The reaction mixture was extracted with $CHCl_3$, and the organic layer was washed with H_2O and dried over anhydrous Na_2SO_4. To this *p*-chloranil (1.23 g, 5 mM) was added, and the mixture was refluxed for 1 h. The reaction mixture subjected to silica gel column chromatography and eluted with $CHCl_3$:hexane (1:1 v/v). The solvent front running brown color band was collected and re-crystallized from $CHCl_3$:hexane afforded pure corrole. The spectroscopic data for these compounds is as follows. TPC: UV-vis (in CH_2Cl_2): λ_{max}, nm (ε $M^{-1}.cm^{-1}$) 646 (8,600) 616 (10,200), 575 (17,100), 415 (1,12,000). TTC: UV-vis (in CH_2Cl_2): λ_{max}, nm (ε $M^{-1}.cm^{-1}$) 649 (9,600) 621 (9,200), 575 (9,700), 418 (1,32,000).

Each sample was subjected to a column chromatographic purification process prior to the NLO measurements. The details of molecular structure and the absorption spectra have been detailed in Figs 1 and 2. All the experiments were performed with the samples dissolved in chloroform and placed in 1-mm glass/quartz cuvette. Picosecond pulses and fs pulses were generated by separate Ti:sapphire lasers (Coherent, Legend amplifiers) operating at a repetition rate of 1 kHz with a pulse durations ~2 ps and ~40 fs at 800 nm. The amplifiers were seeded with ~15 fs pulses from

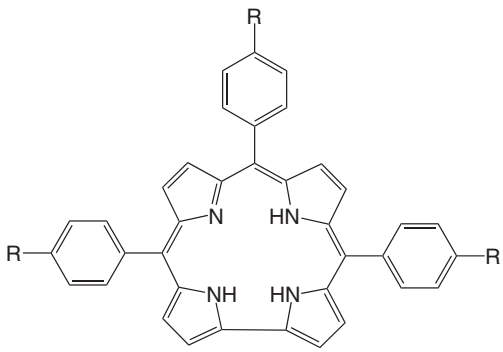

Fig. 1. Structures of corroles used (a) R = H, triphenyl corrole (TPC), molecular formula = $C_{37}H_{26}N_4$; (b) R = -CH_3, tritolyl corrole (TTC), molecular formula = $C_{40}H_{32}N_4$

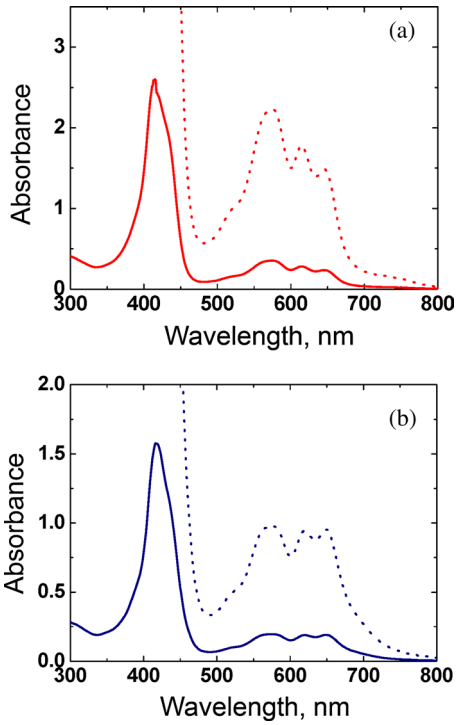

Fig. 2. Absorption spectra of (a) TPC and (b) TTC in chloroform. Dotted lines represent the expanded view

the oscillator (Coherent, Micra). The input beam was spatially filtered to obtain a pure Gaussian profile in the far field. Z-scan studies [19, 24, 29] were performed by focusing the 3-mm diameter input beam using a 200 mm focal length convex lens into the sample in both psec and fsec domains. The sample was placed on a high resolution translation stage and the detector (Si photodiode, SM1PD2A, Thorlabs) output was connected to a lock-in amplifier. Both the stage and lock-in were controlled by a computer program. The picosecond studies were performed with solutions having the concentration of 0.5 mM providing ~75% (for TPC) and ~70% (for TTC) linear transmittance with 800 nm wavelength and picosecond spectral dependent studies were performed with same solution having the same concentration providing ~65% (for TPC) and ~55% (for TTC) linear transmittance at 680, 700 and 740 nm wavelengths. Picosecond studies with 0.25 mM (85% transmittance) were performed with very high peak intensities to completely understand the intensity dependent nonlinear absorption. Femtosecond studies were performed with solutions having concentration of ~1 mM providing 90% linear transmittance at the 800 nm wavelength. Closed aperture scans were performed at intensities where the contribution from the higher order nonlinear effects is negligible (the value of $\Delta\phi$ estimated in all the cases was $<\pi$). The experiments were repeated more than once and the best data were used for obtaining the nonlinear optical coefficients from the best fits. Schematic of the experiment is shown in Fig. 3.

RESULTS AND DISCUSSION

Picosecond NLO studies at 800 nm, 680 nm, 700 nm and 740 nm

Figures 4(a) and 4(b) illustrate the closed aperture Z-scan data recorded at 800 nm for TPC at an intensity of 33 GW/cm^2 and TTC at an intensity of 40 GW/cm^2, well below the peak intensities where the contribution from solvent starts to be significant. Both the samples exhibited negative nonlinearity as discovered by the peak-valley signature. The magnitudes of nonlinear refractive indices (n_2) evaluated, using the standard procedure, were 1×10^{-14} cm^2/W for TPC and 0.6×10^{-14} cm^2/W for TTC, respectively. To determine the irradiance dependence of nonlinear absorption, we performed our measurements at different input laser energies. Figures 5(a) and 5(b) present the obtained intensity dependent Z-scan curves for TPC and TTC. In particular, we noted that the increase of laser intensity induced a switching from saturable

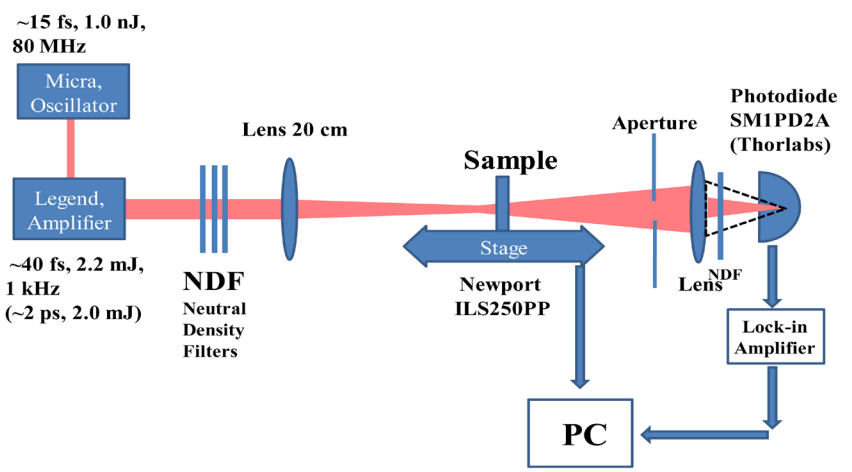

Fig. 3. Experimental schematic of Z-scan

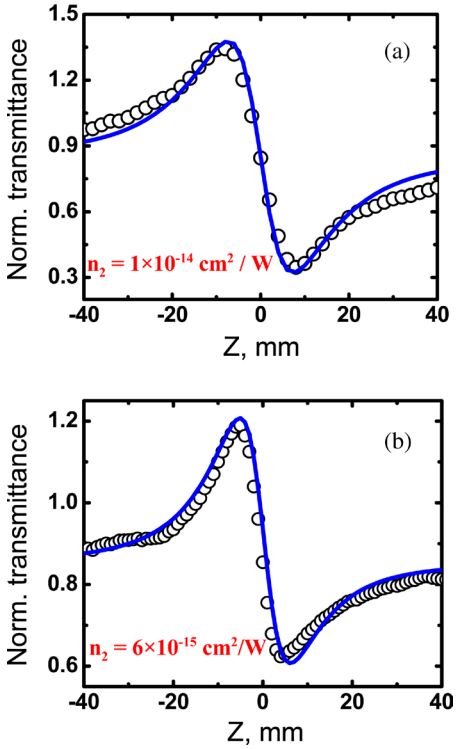

Fig. 4. Closed aperture Z-scan curves (open circles) for (a) TPC with I_{00} = 33 GW/cm^2 and (b) TTC with I_{00} = 40 GW/cm^2 obtained near 800 nm for a concentration of 5 × 10^{-4} M. Solid line is theoretical fit

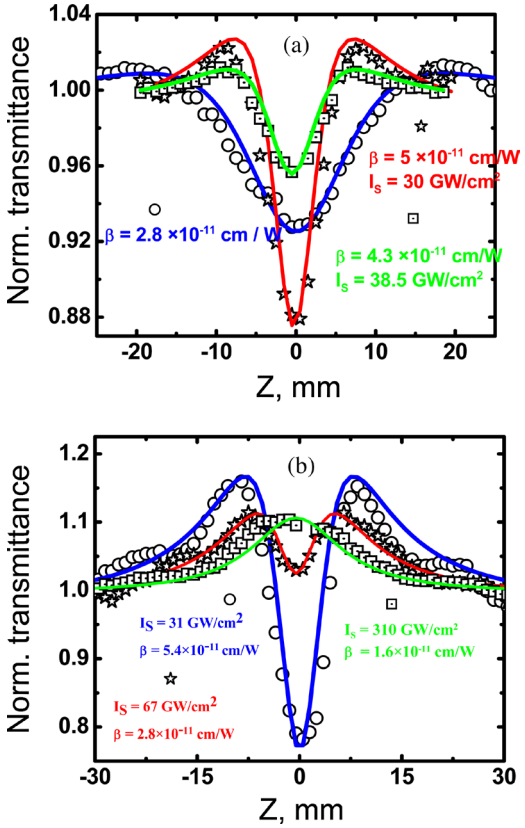

Fig. 5. Open aperture Z-scan curves obtained for (a) TPC with varying input intensities like (open squares) I_{00} = 55 GW/cm^2, (open stars) I_{00} = 93 GW/cm^2 and (open circles) I_{00} = 122 GW/cm^2 (b) TTC with (open squares) I_{00} = 98 GW/cm^2, (open stars) I_{00} = 170 GW/cm^2 and (open circles) I_{00} = 245 GW/cm^2. The concentration used was 5 × 10^{-4} M. Solid line is theoretical fit

absorption (SA) to reverse saturable absorption (RSA) to purely RSA behavior in the case of TPC. For the case of TTC we observed switching from saturable absorption to reverse saturable absorption. In Fig. 5(a) open circles represent the results obtained at high peak intensity of 122 GW/cm^2 which clearly demonstrates pure RSA (2PA). Intriguingly, lower intensity data (open squares at 55 GW/cm^2 and open stars at 93 GW/cm^2, respectively) demonstrates that the nonlinear absorption transformed from SA to RSA. Figure 5(b) shows the Z-scan curves with open squares denoting the data obtained at low peak intensity of 98 GW/cm^2. When the linear absorption is significant and with low peak intensity the transmission increases monotonically (SA) and the same was observed at lower peak intensities. However, for increasing intensities (open circles representing the data at 245 GW/cm^2 and open stars at 170 GW/cm^2, respectively) the nonlinear absorption of sample changed from SA to RSA.

To interpret and fit the data for the flip of saturable absorption around the beam waist, we combined saturable absorption coefficient and two photon absorption (TPA, β) coefficients yielding the total absorption coefficient [30, 31] as;

$$\alpha(I) = \alpha_0 \frac{1}{1+\frac{I}{I_S}} + \beta I \qquad (1)$$

where the first term describes the negative nonlinear absorption and the second term describes positive nonlinear absorption such as reverse saturable absorption and/or two photon absorption α_0 is the linear absorption coefficient. I and I_S are laser peak intensity and saturation intensity, respectively. β is the nonlinear absorption coefficient. In presence of saturable absorption only the intensity dependent nonlinear absorption is given by the equation [31–33];

$$\alpha(I) = \alpha_0 \frac{1}{1+\frac{I}{I_S}} \qquad (2)$$

Using Equations 1 and 2, I_s and β can be obtained from the open aperture Z-scan data by fitting it to the following equation;

$$\frac{dI}{dz'} = -\alpha(I)I \qquad (3)$$

where z′ corresponds to sample length. If the excitation intensity I is lesser than I_s, we can consider SA as a third order process and in such cases $-(\alpha_0/I_s)$ is the equivalent of nonlinear absorption coefficient β (negative nonlinear

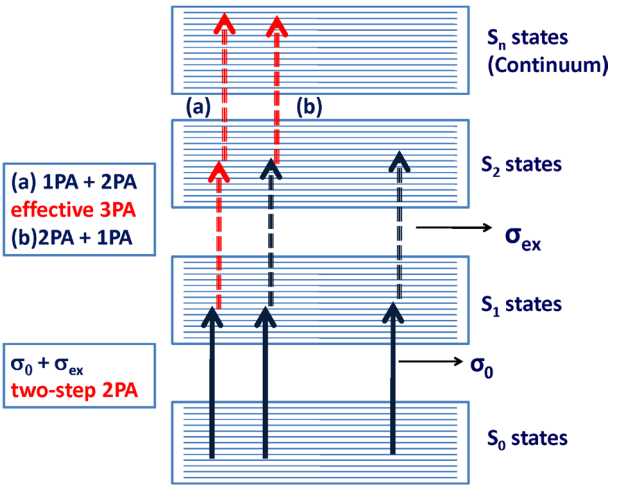

Fig. 6. Energy level diagram of corroles explaining the various nonlinear absorption processes

absorption), to a good approximation. Im $[\chi^{(3)}]$ can be evaluated from β [33]. The observed behavior can be qualitatively explained using the energy level diagram of corroles depicted in Fig. 6. For lower peak intensities the population in the ground state is bleached initially (S_0 states to S_1 states). Further pumping leads to excitation into higher excited singlet states (S_2 state) since the excited state absorption cross-section is significant at higher peak intensities and this is reflected in the switching of SA to RSA. This can be considered as two-step 2PA (β) and the data has been fitted accordingly [33, 34].

SA generally occurs due to depletion of the ground state population and occurs in the regions near resonance. On other hand, RSA is due to further absorption taking place from first or higher excited singlet states. This is also called excited state absorption (ESA). The condition for occurrence of ESA is that the first excited singlet state S_1 should have an absorption cross-section, σ_{ex}, higher than that of ground state absorption cross-section (σ_0) [23]. On the other hand if σ_0 is greater than σ_{ex}, SA is observed. As the wavelength of excitation is shifted closer to (or away from) the wavelength of resonant absorption, σ_0 increases (decreases). Consequently the figure of merit of RSA defined as the ratio σ_{ex}/σ_0, decreases (increases) resulting in a changeover of nonlinear absorption mechanism from RSA to SA (SA to RSA). Wavelength region over which nature of NL absorption changes between RSA and SA is very important for optical limiting applications. It is highly desirable that optical limiter posses broad band response. Figures 7(a)–7(f) show the typical open aperture and closed aperture Z-scan graphs obtained for TPC and TTC samples in the 680–740 nm spectral range. Measured values of I_S, β, n_2, Im $[\chi^{(3)}]$, Re $[\chi^{(3)}]$ and $|\chi^{(3)}|$ at different wavelengths of excitation are provided in Table 1. Both samples, TPC and TTC, exhibited SA from 680–740 nm, except for TTC at 700 nm with higher peak intensities, though their saturation intensity was found to be slightly different. The condition that the excitation intensity should be less than saturation intensity I_S not satisfied in all cases except at 740 nm wavelength. However, at 700 nm, these two samples exhibited different behavior. While TTC showed switching to slight RSA from SA, TPC still exhibited SA. For both the samples I_S was found to increase as the excitation wavelength is shifted away from the resonance.

Figures 8(a) and 8(b) shows the open aperture Z-scan data recorded for both TPC and TTC at a concentration of 0.25 mM clearly illustrating RSA kind of behavior at 800 nm recorded at peak intensity of ~400 GW/cm^2. It is

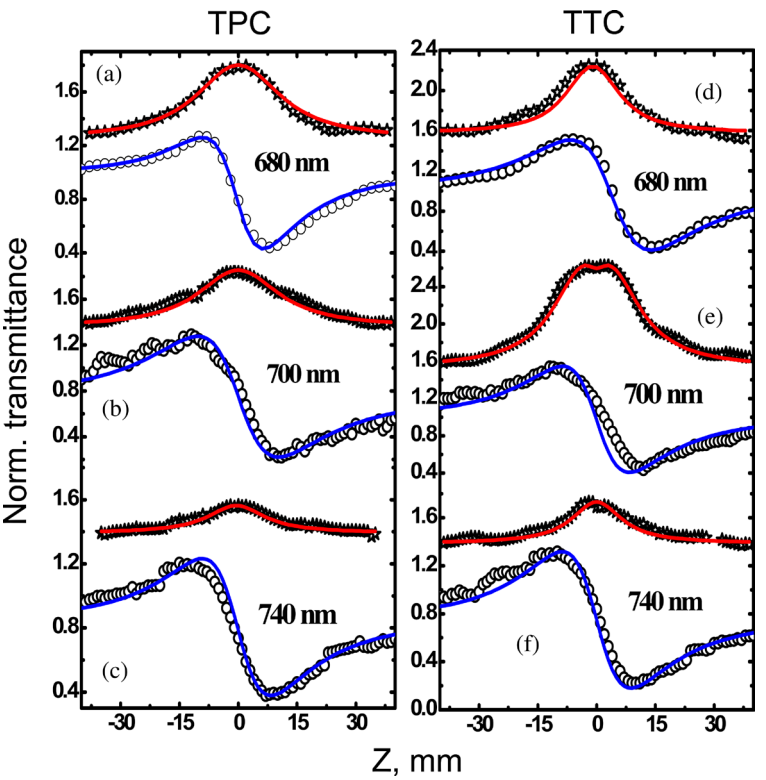

Fig. 7. Z-scan curves (a) open aperture (open stars) and closed aperture (open circles) I_{00} = 57 GW/cm^2 at 680 nm (b) open aperture (open stars) with I_{00} = 72 GW/cm^2 and closed aperture (open circles) with I_{00} = 54 GW/cm^2 at 700 nm and (c) open aperture (open stars) with I_{00} = 90 GW/cm^2 and closed aperture (open circles) with I_{00} = 32 GW/cm^2 at 740 nm for TPC (d) open aperture (open stars) and closed aperture (open circles) with I_{00} = 76 GW/cm^2 at 680 nm (e) open aperture (open stars) with I_{00} = 108 GW/cm^2 and closed aperture (open circles) with I_{00} = 25 GW/cm^2 at 700 nm (f) open aperture (open stars) with I_{00} = 96 GW/cm^2 and closed aperture (open circles) with I_{00} = 25 GW/cm^2 at 740 nm for TTC. The concentration used was 5 × 10^{-4} M. Open aperture data has been shifted for clarity

Table 1. Summary of nonlinear coefficients obtained from the present studies in picosecond domain

Wavelength	Sample	$b \times 10^{-11}$ cm/W	$n_2 \times 10^{-14}$ cm^2/W	$Im[\chi^{(3)}] \times 10^{-21}$ m^2/V^2	$Re[\chi^{(3)}] \times 10^{-20}$ m^2/V^2	$\lvert\chi^{(3)}\rvert \times 10^{-21}$ m^2/V^2	$\lvert\chi^{(3)}\rvert \times 10^{-12}$ (e.s.u.)
800 nm	TPC	2.8 (2PA)	1.0	1.95	1.11	11.31	5.3
	TTC	5.4 (I_S = 31 GW/cm^2)	0.6	3.77	0.66	7.65	3.6
740 nm	TPC	-2.9 (I_S = 200 GW/cm^2)	1.0	-1.87	1.11	11.26	5.3
	TTC	-6.1 (I_S = 150 GW/cm^2)	2.0	-3.94	2.22	22.55	10.6
700 nm	TPC	0 (I_S = 28 GW/cm^2)	0.8	—	—	—	—
	TTC	1.5 (I_S = 8 GW/cm^2)	1.0	0.92	1.11	10.14	5.25
680 nm	TPC	0 (I_S = 16 GW/cm^2)	0.5	—	—	—	—
	TTC	0 (I_S = 35 GW/cm^2)	0.7	—	—	—	—

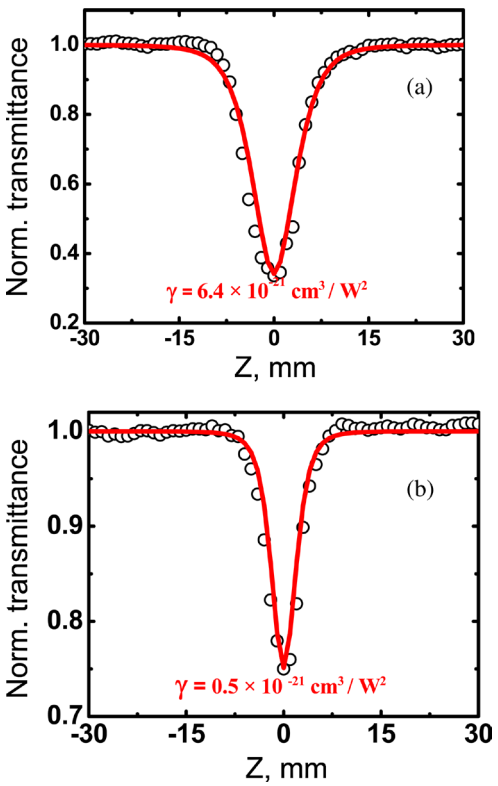

Fig. 8. Open aperture Z-scan curves (open circles) for (a) TPC and (b) TTC obtained near 800 nm for concentration of 2.5×10^{-4} M using an intensity of 350 GW/cm^2. Solid line is theoretical fit

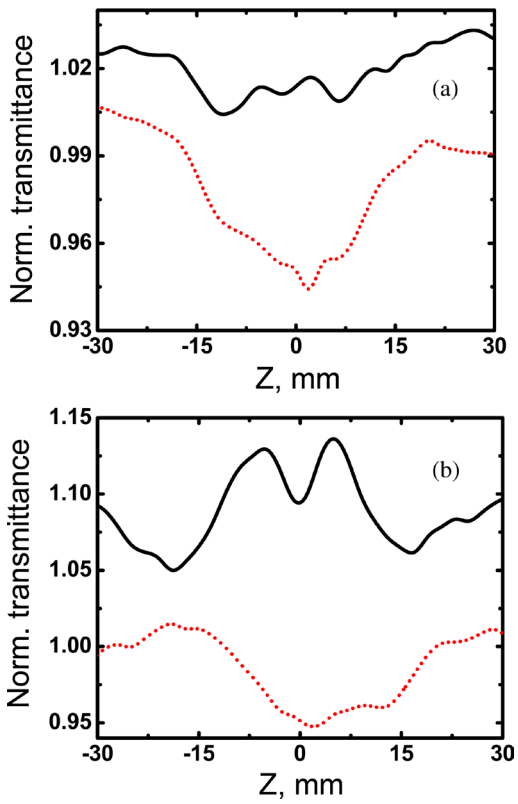

Fig. 9. Open aperture Z-scan curves for (a) TPC with two different intensities 110 GW/cm^2 (dotted line) and 82 GW/cm^2 (solid line) (b) TTC with two different intensities 170 GW/cm^2 (dotted line) and 110 GW/cm^2 (solid line) obtained at 800 nm for concentration of 2.5×10^{-4} M

evident from the theoretical fits [18–20] that three-photon absorption (3PA) is the dominant nonlinear absorption mechanism. The fits yielded values of $\gamma \sim 10^{-21}$ cm^3/W^2. TTC had higher 3PA coefficient compared to TPC. The solvent (chloroform) contribution, though present, was quite small (less than one order of magnitude) compared to the contribution of solute. At lower peak intensities, and with the same concentration, both samples exhibited complex behavior with switching from RSA with in SA, which is as shown in Figs 9(a) and 9(b). Again, this behavior can be explained using the energy level diagram provided in Fig. 6. At lower peak intensities SA is dominant while at moderately high peak intensities switching to RSA is observed due to presence of population in the S_2 state [34]. At very high peak intensities there could be further absorption from S_2 states to S_n states *via* two possible mechanisms depicted by (a) and (b) in Fig. 6. This can be termed as effective 3PA (two-step 3PA). Following the theory provided below [35] we fitted the data using Equation 5 or 6 to obtain and effective 3PA coefficient.

Assuming a spatial and temporal Gaussian profile for laser pulses and utilizing the open aperture Z-scan theory for two photon absorption (2PA) given by Sheik-Bahae *et al.* [29] the equation for 2PA open aperture (OA) normalized power transmittance given by [35, 36];

$$T_{OA}(2PA) = \frac{1}{\pi^{1/2} q_0(z,0)} \int_{-\infty}^{\infty} \ln[1 + q_0(z,0)\exp(\tau^2)]d\tau \quad (4)$$

Three-photon absorption (3PA) equation is;

$$T_{OA}(3PA) = \frac{1}{\pi^{1/2} p_0} \int_{-\infty}^{\infty} \ln\left\{[1 + p_0^2 \exp(-2\tau^2)]^{1/2} + p_0 \exp(-\tau^2)\right\} d\tau \quad (5)$$

For $|p_0| < 1$, and ignoring the higher order terms, we obtain;

$$T_{OA}(3PA) = 1 - 2\gamma I_{00}^2 L'_{eff} \Big/ (1 + (z/z_0)^2)3^{3/2} \quad (6)$$

where;

$$q_0(z,0) = \frac{\beta I_{00} L_{eff}}{1 + (z/z_0)^2}, \qquad p_0(z,0) = \frac{2\gamma I_{00}^2 L'_{eff}}{1 + (z/z_0)^2}$$

I_{00} is the peak intensity, z is the sample position, $z_0 = \pi\varpi_0^2/\lambda$ is the Rayleigh range: ω_0 is the beam waist at the focal point (z = 0), λ is the laser wavelength; effective path length in the sample of length L for 2PA, 3PA is given as .

$$L_{eff} = \frac{1 - e^{-\alpha_0 L}}{\alpha_0}, \quad L'_{eff} = \frac{1 - e^{-2\alpha_0 L}}{2\alpha_0}$$

We have evaluated the three photon cross-section (σ_3) using the relation

$$\sigma_3 = \frac{(\hbar\omega)^2}{N}\gamma \quad (7)$$

where ω is the frequency of the laser radiation, and N is the number density. The cross-section values estimated for TPC and TTC were 25.9 × 10^{-76} $cm^6.s^2$/photon^2 and 2.44 × 10^{-76} $cm^6.s^2$/photon^2, respectively. These values represent one of the highest values reported in recent literature [5, 21, 22]. The values of 2P cross-sections evaluated for TPC and TTC (obtained with ps pulses) were ~10^3 GM. The nonlinear coefficients obtained in this study are comparable to some of the recently reported highly efficient NLO materials [5, 37]. For example, Venugopal Rao *et al.* [37] reported 2PA coefficients in the range of 0.05–0.13 cm/GW and 3PA coefficients in the range of 3.5–20.0 × 10^{-21} cm^3/W^2 for five different porphycenes synthesized recently. Anusha *et al.* [24, 38] observed 2PA with magnitude of 0.1 cm/GW and 0.275 cm/GW in alkoxy and alkyl phthalocyanines using 2 ps pulses at 800 nm. Kumar *et al.* [21, 22] observed 3PA with fs pulse excitation in solutions of alkyl phthalocyanines and estimated a magnitude of ~10^{-22} cm^3/W^2. Srinivas *et al.* [39] reported 2PA in porphyrins over a range of wavelengths in the visible spectral region with their magnitudes of ~1 cm/GW but the data was obtained with ns pulses. Venkatram *et al.* [23] reported large 2PA coefficients in the range of 2000 cm/GW for alkoxy phthalocyanines with 532 nm ns pulses. The coefficients are expected to be larger in the ns regime while in the ps/fs regime the nonlinearities are comparatively smaller. However, the figures of merit obtained for our molecules demand further study on the time response of these nonlinearities.

NLO studies with 800 nm, ~40 fs pulses

Open aperture scans for TPC and TTC recorded at 800 nm using ~40 fs pulses indicated SA apparent from the changes in transmittance values. The concentrations of solutions were ~1 mM. Figures 10(a) and 10(b) illustrate the open aperture data (stars) obtained with

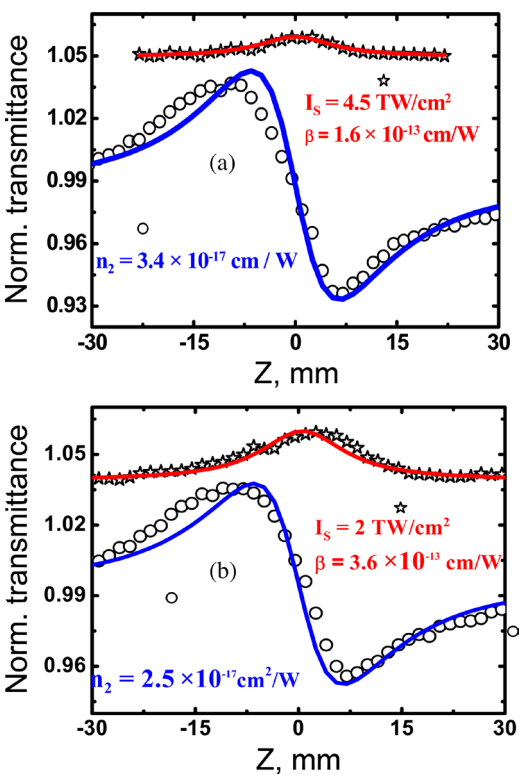

Fig. 10. (a) Fs open aperture for TPC with I_{00} = 0.7 TW/cm^2 (open stars) and closed aperture (open circles) with I_{00} = 1.0 TW/cm^2 and (b) Fs open aperture for TTC with I_{00} = 0.7 TW/cm^2 (open stars) and closed aperture with I_{00} = 1.0 TW/cm^2 (open circles) obtained at 800 nm for a concentration of 1 × 10^{-3} M. Open aperture data has been shifted up for clarity

Table 2. Summary of nonlinear coefficients obtained from the present studies using fs pulses

Sample	β(fs) $\times 10^{-13}$ cm/W	n_2(fs) $\times 10^{-17}$ cm^2/W	Im[$\chi^{(3)}$] $\times 10^{-23}$ m^2/V^2	Re[$\chi^{(3)}$] $\times 10^{-23}$ m^2/V^2	$\lvert\chi^{(3)}\rvert \times 10^{-23}$ m^2/V^2	$\lvert\chi^{(3)}\rvert \times 10^{-14}$ (e.s.u)
TPC	-1.6	3.4	-1.12	3.77	3.94	1.9
TTC	-3.6	2.5	-2.51	2.78	3.74	1.8

an intensity of 0.7 TW/cm^2 and closed aperture data (open circles) with an intensity of 1.0 TW/cm^2. The peak intensities were calculated considering the pulse duration to be ~70 fs due to broadening from the optical components (neutral density filters and lenses). An independent experiment performed for measuring the pulse duration indeed confirmed the value to be 70–75 fs. The experiment was performed using Silhouette (Coherent, USA) with optical components in the path. The data was recorded for TPC and TTC well below the intensity levels where the contribution from solvent is significant. Obtained experimental data was fitted using Equations 2 and 3. We found the best fit was obtained with transmittance equation for SA. The fs pulses possess large bandwidth (~26 nm) and in combination with linear absorption at 800 nm we can only expect saturation of the S_1 state. For pumping with higher peak intensities we observed Supercontinuum generation from the solvent. Both the samples exhibited negative nonlinearity as discovered by the peak-valley signature in the fs domain also. The magnitudes of the nonlinear refractive indices (n_2) evaluated, using the standard procedure, were 3.4×10^{-17} cm^2/W for the TPC and 2.5×10^{-17} cm^2/W for TTC. The summary of NLO coefficients is presented in Table 2. The solvent nonlinearity was positive suggesting the final values of n_2 calculated for the pure solute will be higher than the calculated. Our future endeavor is to study the (1) fs NLO properties of these molecules at different wavelengths in the visible and NIR (2) excited state dynamics of both the molecules using ultrafast pump-probe techniques (3) incorporate these molecules in suitable polymer/glass matrix and later evaluate their NLO properties and dynamics.

CONCLUSION

In summary, the changeover from saturable absorption to reverse saturable absorption in both samples was investigated at the wavelength of 800 nm with 5×10^{-4} M in picosecond domain. It was found that the sample TTC demonstrated saturable absorption at low intensities, with switching from reverse saturable absorption within saturable absorption at high intensities and TPC depicted switching from RSA within SA at lower intensities to pure RSA (TPA) at higher intensities. The shift was analyzed phenomenologically in terms of an intensity-dependent saturable absorption and reverse saturable absorption. We have also investigated the 2 ps spectral dependent Z-scan studies. At 700 nm TPC exhibited predominantly SA while RSA within SA was observed in TTC. Since the structural difference between these two samples is only TPC (R = -CH_3) and TTC (R = -H), observed difference in the wavelength dependence of their nonlinear absorption can be due to varying influence of this difference. We have also carried out Z-scan studies with 800 nm, ~40 fs pulses and characterized the nonlinearities in detail. From the fs open aperture data we derived that these molecules exhibit saturable absorption (SA) behavior. Both the samples exhibited negative nonlinear refractive index in both the time domains of investigation. In some of the cases we observed peak intensity being lesser than saturation intensity and we calculated nonlinear absorption coefficients. We measured the values of I_S, β, n_2, Im [$\chi^{(3)}$], Re [$\chi^{(3)}$] and $|\chi^{(3)}|$ for all wavelengths.

Acknowledgements

S. Venugopal Rao acknowledges the financial support from DRDO. SH acknowledges the constant support of Ms. P.T. Anusha and Mr. P. Gopala Krishna during the entire course of experimental work. LG acknowledges the financial support from DST.

REFERENCES

1. Senge MO, Fazekas M, Notaras EGA, Blau WJ, Zawadzka M, Locos OB and Ni Mhuircheartaigh EM. *Adv. Mater*. 2007; **19**: 2737–2774.
2. de la Torre G, Vazquez P, Agullo-Lopez F and Torres T. *Chem. Rev*. 2004; **104**: 3723–3750.
3. Vagin S, Barthel M, Dini D and Hanack M. *Inorg. Chem*. 2003; **42**: 2683–2694.
4. Calvete M, Yang GY and Hanack M. *Synth. Met*. 2004; **141**: 231–243.
5. Sarma T, Panda PK, Anusha PT and Venugopal Rao S. *Org. Lett.* 2010; **13**: 188–191 and references therein.
6. Arnbjerg J, Ana JB, Martin JP, Nonell S, Borrell JI, Christiansen O and Ogilby PR. *J. Am. Chem. Soc.* 2007; **129**: 5188–5199.
7. Flamigni L and Gryko DT. *Chem. Soc. Rev*. 2009; **38**: 1635–1646.
8. D'Souza F, Chitta R, Ohkubo K, Tasior M, Subbaiyan NK, Zandler ME, Rogacki MK, Gryko DT and Fukuzumi S. *J. Am. Chem. Soc.* 2008; **130**: 14263–14272.

9. Wasbotten IH, Wondimagegn T and Ghosh A. *J. Am. Chem. Soc.* 2002; **124**: 8104–8115.
10. Shetti VS, Prabhu UR and Ravikanth M. *J. Org. Chem*. 2010; **75**: 4172–4182.
11. Sankar J, Rath H, Prabhu Raja V, Chandrashekar TK and Vittal JJ. *J. Org. Chem.* 2004; **69**: 5135–5138.
12. Narayanan N, Sridevi B and Chandrashekar TK. *Org. Lett.* 1999; **1**: 587–590.
13. Rebane A, Drobizhev M, Makarov NS, Koszarna B, Tasior M and Gryko DT. *Chem. Phys. Lett.* 2008; **462**: 246–250.
14. Rebane A, Makarov N, Drobizhev M, Koszarna B, Galezowski M and Gryko DT. *Proc. SPIE* 2009; **7213**: 72130Q-1.
15. Cho S, Lim JM, Hiroto S, Kim P, Shinokubo H, Osuka A and Kim D. *J. Amer. Chem. Soc.* 2009; **131**: 6412–6420.
16. Venugopal Rao S, Srinivas NKMN, Giribabu L, Maiya BG, Rao DN, Philip R and Kumar GR. *Opt. Commun.* 2000; **182**: 255–264.
17. Venugopal Rao S, Srinivas NKMN, Giribabu L, Maiya BG, Rao DN, Philip R and Kumar GR. *Opt. Commun.* 2001; **192**: 123–133.
18. Venugopal Rao S and Rao DN. *J. Porphyrins Phthalocyanines* 2002; **6**: 234–237.
19. Venugopal Rao S, Anusha PT, Prashant TS, Swain D and Tewari SP. *Mater. Sci. Appl.* 2011; **2**: 299–306.
20. Venugopal Rao S, Swain D and Tewari SP. *Proc. SPIE* 2010; **7599**: 75991P.
21. Kumar RSS, Venugopal Rao S, Giribabu L and Rao DN. *Chem. Phys. Lett.* 2007; **447**: 274–278.
22. Kumar RSS, Venugopal Rao S, Giribabu L and Rao DN. *Proc. SPIE* 2008; **6875**: 68751D.
23. Venkatram N, Giribabu L, Rao DN and Venugopal Rao S. *Appl. Phys. B* 2008; **91**: 149–156.
24. Anusha PT, Reeta PS, Giribabu L, Tewari SP and Venugopal Rao S. *Mater. Lett.* 2010; **64**: 1915–1917.
25. Venugopal Rao S. *Proc. SPIE* 2010; **7728**: 77281N.
26. Mathews SJ, Kumar SC, Giribabu L and Venugopal Rao S. *Opt. Commun*. 2007; **280**: 206–212.
27. Mathews SJ, Kumar SC, Giribabu L and Venugopal Rao S. *Mat. Lett.* 2007; **61**: 4426–4431.
28. Koszarna B and Gryko DT. *J. Org. Chem.* 2006; **71**: 3707–3717.
29. Sheik-Bahae M, Said AA, Wei TH, Hagan DJ and Van Stryland EW. *IEEE J. Quant. Electron.* 1990; **26**: 760–769.
30. Gao Y, Zhang X, Li Y, Liu H, Wang Y, Chang Q, Jiao W and Song Y. *Opt. Commun.* 2005; **251**: 429–433.
31. Samoc M, Samoc A, Davies BL, Reisch H and Scherf U. *Opt. Lett.* 1998; **23**: 1295–1297.
32. Kandasamy K, Rao KD, Deshpande R, Puntambekar PN, Singh BP, Shetty SJ and Srivastava TS. *Appl. Phys. B* 1997; **64**: 479–484.
33. Unnikrishnan KP, Thomas J, Nampoori VPN and Vallabhan CPG. *Opt. Commun*. 2003; **217**: 269–274.
34. Venkatram N, Rao DN, Giribabu L and Venugopal Rao S. *Chem. Phys. Lett*. 2008; **464**: 211–215.
35. Gu B and Ji W. *Opt. Exp*. 2008; **16**: 10208–10213.
36. Saravanan KV, Raju KCJ, Krishna MG, Tewari SP and Venugopal Rao S. *Appl. Phys. Lett.* 2010; **96**: 232905–232908.
37. Venugopal Rao S, Prashant TS, Swain D, Sarma T, Panda PK and Tewari SP. *Chem. Phys. Lett.* 2011; **514**: 98–103.
38. Anusha PT, Reeta PS, Giribabu L, Tewari SP and Venugopal Rao S. *Pramana* 2010; **75**: 1017–1023.
39. Srinivas NKMN, Venugopal Rao S, Rao DVGLN, Kimball BK, Nakashima M, Decristofano BS and Rao DN. *J. Porphyrins Phthalocyanines* 2001; **5**: 549–554.